

In-Situ Switching from Barrier-Limited to Ohmic Anodes for Efficient Organic Optoelectronics

Zhi-Kuang Tan, Yana Vaynzof, Dan Credgington, Cheng Li, Mike T. L. Casford, Alessandro Sepe, Sven Huettner, Mark Nikolka, Fabian Paulus, Le Yang, Henning Sirringhaus, Neil C. Greenham, and Richard H. Friend*

Injection and extraction of charges through ohmic contacts are required for efficient operation of semiconductor devices. Treatment using polar non-solvents switches polar anode surfaces, including PEDOT:PSS and ITO, from barrier-limited hole injection and extraction to ohmic behaviour. This is caused by an in-situ modification of the anode surface that is buried under a layer of organic semiconductor. The exposure to methanol removes polar hydroxyl groups from the buried anode interface, and permanently increases the work function by 0.2–0.3 eV. In the case of ITO/PEDOT:PSS/PBDTTT-CT:PC71BM/Al photovoltaic devices, the higher work function promotes charge transfer, leading to p-doping of the organic semiconductor at the interface. This results in a two-fold increase in hole extraction rates which raises both the fill factor and the open-circuit voltage, leading to high power conversion efficiency of 7.4%. In ITO/PEDOT:PSS/F8BT/Al polymer light-emitting diodes, where the organic semiconductor's HOMO level lies deeper than the anode Fermi level, the increased work function enhances hole injection efficiency and luminance intensity by 3 orders of magnitude. In particular, hole injection rates from PEDOT:PSS anodes are equivalent to those achievable using MoO₃. These findings exemplify the importance of work function control as a tool for improved electrode design, and open new routes to device interfacial optimization using facile solvent processing techniques. Such simple, persistent, treatments pave the way towards low cost manufacturing of efficient organic optoelectronic devices.

organic electronic devices. A large work function difference between the anode and the cathode of an organic solar cell is required to create a strong built-in potential for assisting carrier transport and for generating a high open-circuit voltage.^[1,2] A high work function anode and a low work function cathode are also required to effectively inject holes and electrons, respectively, into organic light emitting diodes.^[3] Scientists and engineers have, traditionally, relied on thin interlayers of calcium^[4] or lithium fluoride^[5] for ohmic electron injection. Recent developments in polyamine surface modifiers have also provided a simple and universal method to achieve low work function electrodes for good electron injection.^[6] To obtain hole-selective ohmic contacts, transition metal oxides with a deep Fermi-level, such as molybdenum trioxide^[7–11] and tungsten trioxide,^[12] are typically utilized as interfacial modifiers. Most commonly, PEDOT:PSS has been used as a solution processable hole injection layer, but its work function is often insufficiently deep for efficient injection into electroluminescent devices.

1. Introduction

Ohmic contacts with sufficiently deep or shallow work functions play an important role in the efficient functioning of

Recent efforts in electrode engineering have culminated in a series of reports, claiming that the insertion of a solution-processed polyelectrolyte layer beneath the metallic cathode was capable of enhancing the performances of organic photovoltaic devices^[13–16] and organic light emitting diodes.^[17] The presence of a small interfacial dipole at the polyelectrolyte/cathode interface has been cited many times as the reason for enhanced device performances. There is, however, growing evidence that the polar solvent used in the polyelectrolyte processing is responsible for much of the performance enhancement.^[18–21] The mechanism behind solvent-induced device enhancement has remained poorly understood with a range of mechanisms cited, including changes in photoactive layer morphology,^[19] dipole creation at the organic/cathode interface,^[18] and surface trap passivation and increased hole mobility.^[21]

In this paper, we show that methanol treatment can be a general method to enhance the hole injection and hole extraction properties in polymer solar cells and light emitting diodes. We further demonstrate that such methanol-induced

Z.-K. Tan, Dr. Y. Vaynzof, Dr. D. Credgington,
C. Li, Dr. A. Sepe, Dr. S. Huettner, M. Nikolka,
F. Paulus, L. Yang, Prof. H. Sirringhaus,
Prof. N. C. Greenham, Prof. R. H. Friend
Cavendish Laboratory
University of Cambridge
JJ Thomson Avenue, Cambridge, CB3 0HE, UK
E-mail: rhf10@cam.ac.uk



Dr. M. T. L. Casford
Department of Chemistry
University of Cambridge
Lensfield Road, Cambridge, CB2 1EW, UK

This is an open access article under the terms of the Creative Commons Attribution License, which permits use, distribution and reproduction in any medium, provided the original work is properly cited.

DOI: 10.1002/adfm.201303426

enhancement is caused by an in-situ modification of the anode surface, buried under a layer of organic semiconductor. Using a combination of device studies, ultraviolet photoelectron spectroscopy (UPS) and electroabsorption (EA) spectroscopy techniques, we establish that the performance enhancement originates from an increase in the anode work function, thereby giving hole-selective ohmic contacts towards the organic semiconductors. We show, using infrared spectroscopy, that the increase in work function is related to the removal of hydroxyl groups at the polar substrate interface.

2. Results and Discussions

In our non-solvent treatment studies, we used a blend of small bandgap polymer PBDTTT-CT (poly[[4,8-bis-(2-ethyl-hexyl-

thiophene-5-yl)-benzo[1,2-b:4,5-b']dithiophene-2,6-diyl]-alt-[2-(2'-ethyl-hexanoyl)-thieno[3,4-b]thiophen-4,6-diyl]]) and PC71BM ([6,6]-phenyl-C71-butyric acid methyl ester) as our model system for photovoltaic devices.^[22] Exposure of an uncapped ITO/PEDOT:PSS/PBDTTT-CT:PC71BM substrate to methanol results in an increase of device open-circuit voltage (V_{oc}) from 0.73 V to 0.78 V and the fill factor from 49% to 56%, thereby increasing the power conversion efficiency from 6.2% to 7.4% (see **Figure 1a**). Remarkably, a huge improvement in performance is also observed on devices using bare ITO as the anode. All the key performance parameters improved on the methanol treated ITO-only device, with V_{oc} improving from 0.46 V to 0.67 V, J_{sc} from 14.3 to 15.8 mA cm^{-2} and fill factor from 39% to 49%. Power conversion efficiency in the ITO-only device was significantly higher at 5.2% after methanol treatment, compared to only 2.5% on the control device. Similar device

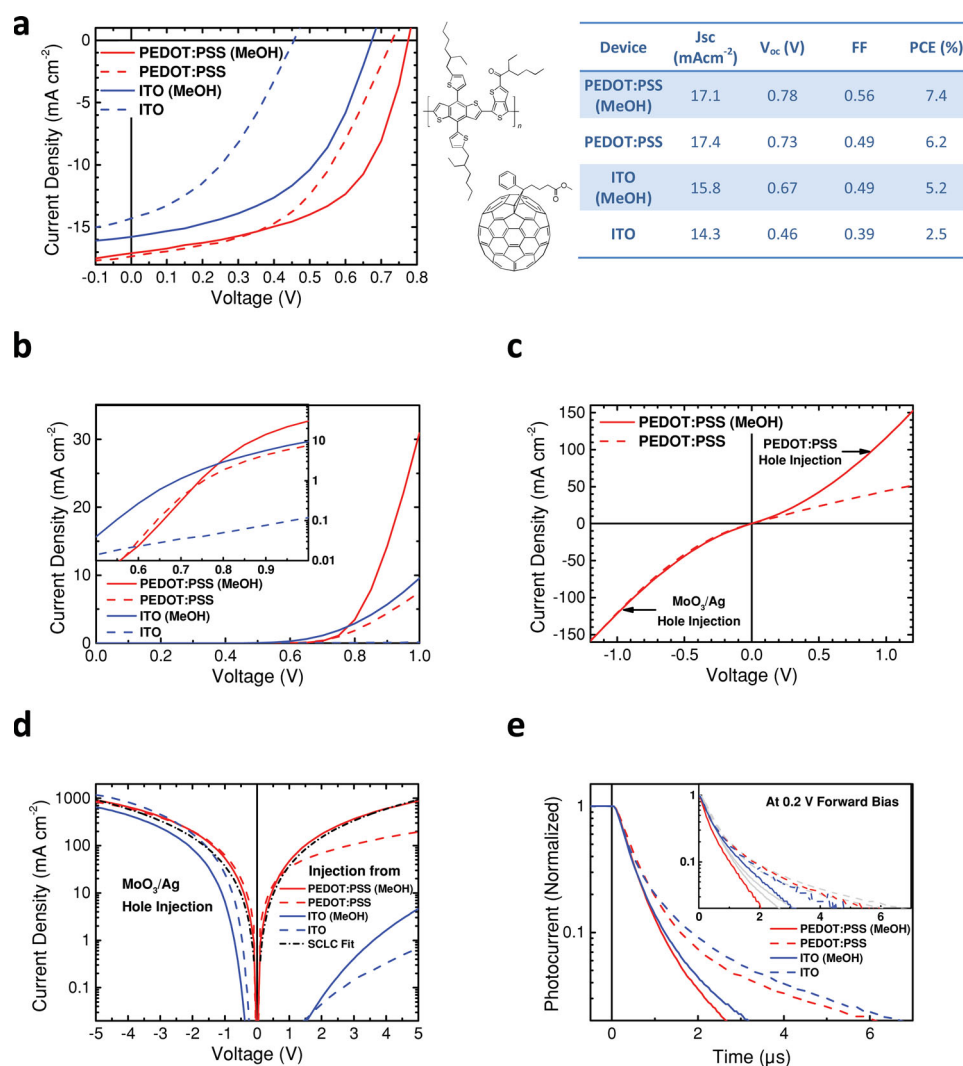


Figure 1. Current density versus voltage characteristics of ITO/PEDOT:PSS/PBDTTT-CT:PC71BM/Al and ITO/PBDTTT-CT:PC71BM/Al devices (a) under simulated AM1.5G illumination, (b) in dark. (c) Current density versus voltage characteristics of ITO/PEDOT:PSS/PBDTTT-CT:PC71BM/MoO₃/Ag hole-only devices. (d) Current density versus voltage characteristics of ITO/PEDOT:PSS/PBDTTT-CT/MoO₃/Ag and ITO/PBDTTT-CT/MoO₃/Ag hole-only devices with SCLC curve fit. (e) Normalized transient photocurrent response of PBDTTT-CT:PC71BM photovoltaic devices under a 10 μs , 525 nm square light pulse, showing photocurrent decay after the pulse is switched off. The inset shows transient photocurrent response of the photovoltaic devices at 0.2 V forward bias. The short-circuit measurements are plotted in grey within the inset for easy comparison.

enhancements can also be achieved using acetonitrile for non-solvent treatment (see Figure S1).^[20]

As shown in Figure 1b, the dark injection currents of both ITO and PEDOT:PSS devices at forward bias were seen to increase significantly with methanol treatment, suggesting either improved bulk carrier mobilities or an improvement in charge injection efficiency. To decouple the effects of charge mobility and injection efficiency, we fabricated hole-only devices with the following device structure: ITO/PEDOT:PSS/PBDTTT-CT:PC71BM/MoO₃/Ag. As shown in Figure 1c, the hole current density significantly increased (up to 3 times) for methanol treated devices when injected from the ITO/PEDOT:PSS electrode, but remained the same when injected from the MoO₃/Ag top electrode. This asymmetric improvement confirms that the increase in hole current density is due to improved injection efficiency of the PEDOT:PSS electrode, and not from an enhancement in bulk hole mobility of the photoactive blend.

Hole-only devices incorporating pure PBDTTT-CT polymer (without PC71BM) reveal that ohmic injection can be achieved from a PEDOT:PSS electrode by simple methanol treatment. As shown in Figure 1d, the hole current from the methanol treated PEDOT:PSS device follows a space-charge limited current (SCLC) relationship,^[23,24] and is completely symmetrical with the injection current from MoO₃, a known ohmic hole injector.^[8–10] It is also clear that methanol treatment improved the hole injection current for both the ITO anode and the PEDOT:PSS anode by nearly an order of magnitude, compared to the control devices. This enhanced hole injection can be effectively retained at ambient conditions over a long period of time, as shown by J-V measurements of the hole-only devices after 9 weeks of storage (see Figure S2).

The device studies above indicate that improved device performance most likely originates from favorable changes at the buried anode/semiconductor interface upon methanol treatment. To confirm that the device enhancements were not related to morphological changes in the photo-active layer, we performed detailed structural characterization using GIWAXS (Figure S3) and GISAXS (Figure S4), surface characterization using AFM (Figure S5) and optical characterization using UV-visible spectroscopy (Figure S6). In these experiments, no observable differences were found between the methanol-treated films and the non-treated films, indicating that the device improvements could not have come from morphological changes, better phase separation, or from the enhanced aggregation of the active layer components. We also performed X-ray photoelectron spectroscopy (XPS) on the methanol-treated films (Figure S7). No changes in chemical composition were detected on the film surface, confirming that methanol treatment has minimal influence on the organic semiconductor surface where the cathode is later deposited.

In order to better understand the origins of improved photovoltaic performance, we performed transient photocurrent experiments on methanol treated devices. In the transient photocurrent experiments, the device at short-circuit condition is illuminated with a 10 μ s square light pulse, during

which a steady state population of charges is built up in the device. The decay of the photocurrent was observed after the pulse is turned off. Since our devices work very efficiently with negligible recombination at short-circuit, the decay of the photocurrent is limited by the rate of charges leaving the device. As detailed above, the primary role of methanol treatment is to alter the anode/semiconductor interface, meaning that changes in the photocurrent transients can be assigned to a change in hole extraction rates. As shown in Figure 1e, the hole extraction rate is twice as fast in both the methanol treated PEDOT:PSS and ITO devices, compared to the control devices. We also measured the photocurrent transients under a 0.2 V forward bias (see inset of Figure 1e), to simulate the effect of a change in the devices' built-in field (see sections below). The photocurrent decay rates at 0.2 V forward bias are very similar to the rates at short-circuit, indicating that the residence time of charge carriers in the devices is primarily limited by the interfacial charge extraction rates rather than by field-driven charge transport within the bulk active layer. This is important as anodes are often assumed to be completely permeable to holes, and charge transport has frequently been considered to be the key factor determining charge density and bimolecular recombination.

An enhanced hole extraction rate at the semiconductor/anode interface will reduce/avoid the accumulation of holes near the anode, therefore preventing the screening of the internal field as well as suppressing bimolecular recombination.^[25,26] The depletion of holes near the anode via improved extraction rates also enhances diffusive transport by establishing a hole density gradient. The reduction of charge recombination and improved transport enable higher photocurrent collection yield across the forward bias regime, and manifests itself as an improved fill factor and higher power conversion efficiency for the solar cell.

Organic photovoltaic devices provide an excellent platform for studying the influence of hole extraction rates on device performance. However, to better examine the effect of methanol treatment on charge injection, we turn to measurements of polymer light emitting diodes (PLEDs). We employed the well-studied green emitter (poly[(9,9-di-n-octylfluorenyl-2,7-diyl)-alt-(benzo[2,1,3]thiadiazol-4,8-diyl)]) (F8BT) as the light emitting polymer (LEP) in a simple ITO/PEDOT:PSS/F8BT/Al configuration.

Figure 2a presents combined current and luminescence measurements of F8BT PLED devices, using PEDOT:PSS as the

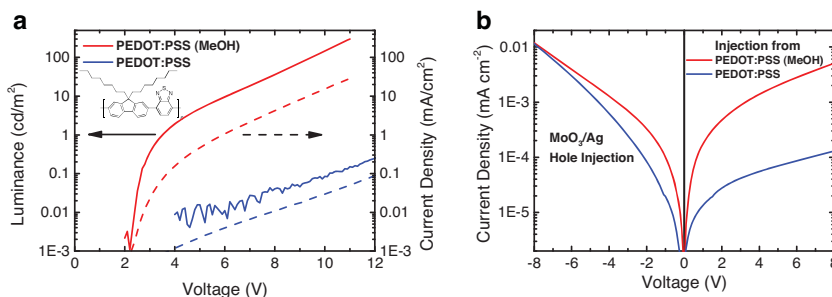


Figure 2. (a) Combined current density (dash line) and luminescence (solid line) versus voltage characteristics of ITO/PEDOT:PSS/F8BT/Al PLED devices. (b) Current density versus voltage characteristics of ITO/PEDOT:PSS/F8BT/MoO₃/Ag hole-only devices.

hole injecting anode. The device current density under forward bias was improved by nearly 3 orders of magnitude upon methanol treatment. The electroluminescence intensity correspondingly increased by 3 orders of magnitude with methanol treatment, achieving a luminescent efficiency of over 1 cd/A after turn-on. Luminescence onset was achieved at approximately 2.5 V for the methanol treated device, while only weak electroluminescence intensity (~ 0.1 cd/m²) was observed for the control device, even at driving voltages exceeding 10 V. No electroluminescence or charge injection was seen for ITO/F8BT/Al devices (without PEDOT:PSS) due to the large hole and electron injection barriers into F8BT.

To study the improvements in hole injection, we fabricated hole-only devices with an ITO/PEDOT:PSS/F8BT/MoO₃/Ag configuration. As can be seen in Figure 2b, the hole injection from PEDOT:PSS improved by 2 orders of magnitude upon methanol treatment. It is typically challenging to attain ohmic hole injection into the deep-lying HOMO (5.95 eV) of F8BT, and the only reported method to achieve this is via the use of high work function MoO₃.^[8–10] The near-symmetric profiles

for hole injection in the methanol-treated PEDOT:PSS device indicate that the treated PEDOT:PSS can inject nearly as well as MoO₃.

The concurrent improvements in hole injection efficiency and electroluminescence intensity demonstrate that efficient hole injection leads in turn to enhanced electron injection from the (normally poor) Al cathode. The high density of injected holes in the semiconductor layer intensifies the electric field near the cathode interface and facilitates the injection of electrons into the semiconductor.^[9,27] This is analogous to the effect seen when employing ohmic cathodes, such as Ca, with (normally poor) PEDOT:PSS anodes, whereby increasing the electron density intensifies the electric field at the anode, sufficient to promote hole injection.^[28,29]

Ultraviolet photoelectron spectroscopy (UPS) measurements on the polymer films and their anode substrates reveal that the improved hole injection/extraction properties, upon methanol treatment, were the result of an increase in the anode work function. As shown by the secondary photoemission onsets in Figure 3a,d, the work function of PEDOT:PSS increased from 5.2

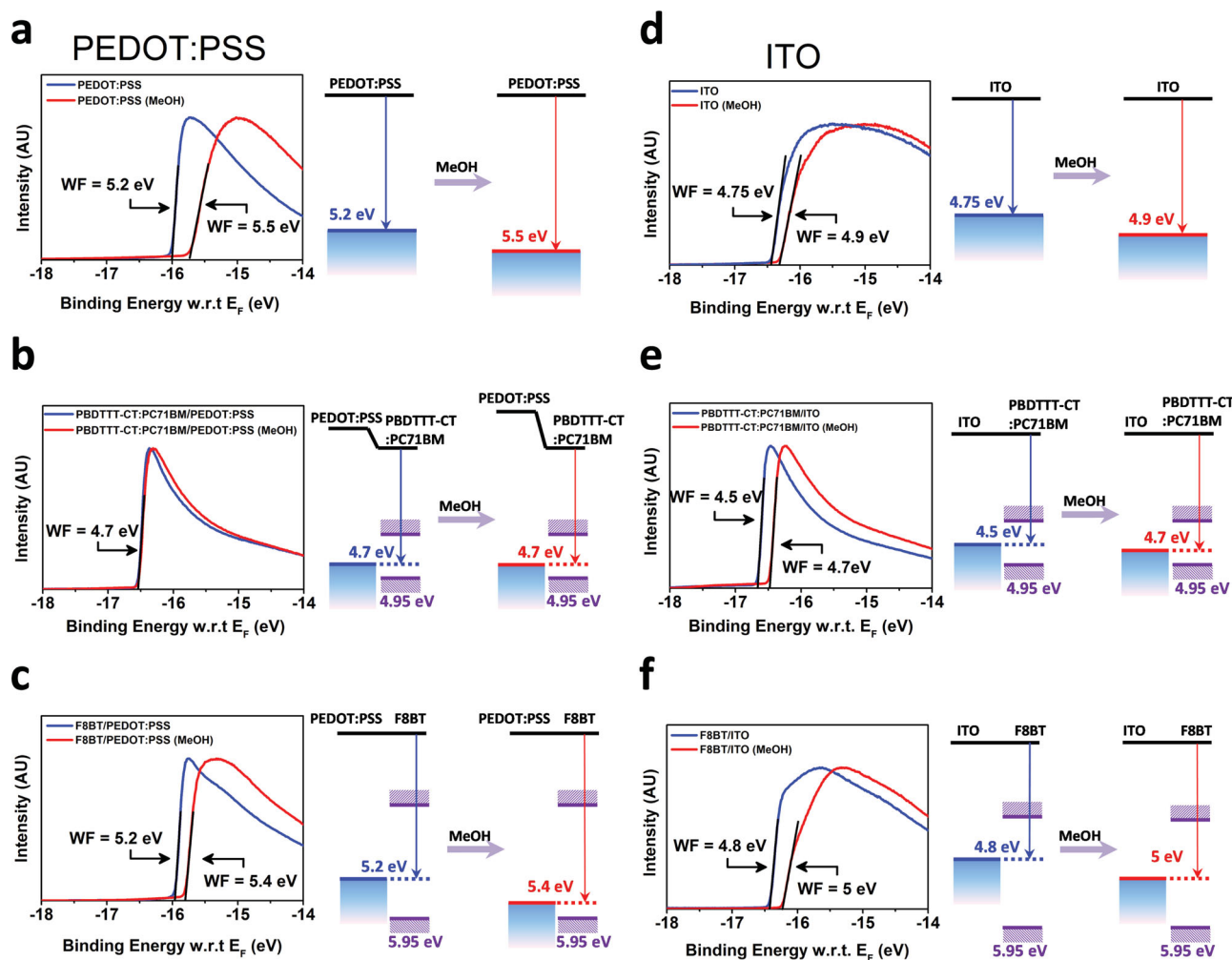


Figure 3. Secondary photoemission onsets of (a) PEDOT:PSS, (b) PBDTTT-CT:PC71BM/PEDOT:PSS, (c) F8BT/PEDOT:PSS, (d) ITO, (e) PBDTTT-CT:PC71BM/ITO and (f) F8BT/ITO with (red) and without (blue) methanol treatment.

eV to 5.5 eV and that of ITO increased from 4.75 eV to 4.9 eV upon methanol treatment. We took extra care to perform the UPS measurements immediately after the methanol treatment to prevent contaminants from affecting the substrate work functions.

Figures 3b and c show the photoemission onsets for PBDTTT-CT:PC71BM and F8BT films deposited on PEDOT:PSS, with and without methanol treatment; and Figures 3e and f show the photoemission onsets of the polymers deposited on bare ITO. Interestingly, we observe a consistent 0.2 eV increase in the work function of the organic films upon methanol treatment, with the exception of PBDTTT-CT:PC71BM/PEDOT:PSS (see Figure 3b). In this case, the Fermi level of the PEDOT:PSS substrate is deeper than the ionization potential of PBDTTT-CT polymer (4.95 eV), which results in spontaneous hole transfer from PEDOT:PSS into PBDTTT-CT and a Fermi level pinning at 4.7 eV. Fermi level pinning will be accompanied by a dipole (or a space-charge region) in the organic semiconductor layer, near the anode/semiconductor interface, as a result of the hole transfer.^[2,30–32] Since the Fermi level is pinned, an increase in the PEDOT:PSS work function by methanol treatment would increase hole transfer (into PBDTTT-CT:PC71BM layer) and consequently intensify the dipole near the interface (see energy-band diagram in Figure 3b). We consider that the improved hole extraction rates in the PBDTTT-CT:PC71BM photovoltaic devices arise from the intensification of this surface field, which effectively sweeps holes into the anode, and reflects surface electrons back into the bulk of the organic semiconductor layer. This makes the treated anode a particularly good hole-selective contact, which reduces surface recombination and enhances diffusive transport, as discussed in the previous section.

For the other samples, the increase in work function is within the Schottky–Mott limit (vacuum level alignment) and the work function of the organic layer reflects that of its underlying substrate. The ionization potential of F8BT (5.95 eV) is too deep to allow spontaneous hole transfer from PEDOT:PSS or ITO, and Fermi level pinning is therefore not observed. The improved hole injection into F8BT, in the methanol treated PLED devices, is therefore given by the reduction in hole injection barrier from the higher work function PEDOT:PSS anode (see energy-band diagram in Figure 3c), and this directly correlates to the improvements in luminance intensity in the PLED devices. The above results clearly indicate that methanol treatment is capable of modifying the work function of the buried substrate in-situ, by penetrating through the over-lying layer of organic semiconductor. However, we note that we have only tested overlayer thicknesses of up to 200 nm, and the effectiveness of methanol treatment on much thicker films is a subject of further investigation.

The hole transfer from PEDOT:PSS into PBDTTT-CT, during Fermi level pinning, p-dopes the semiconducting polymer near the interface. We confirm the presence of hole doping in PBDTTT-CT:PC71BM photovoltaic devices using electroabsorption (EA) spectroscopy. This technique is typically used to estimate the built-in potential of a device by measuring the Stark shift in the semiconductor absorption, produced by a modulation of the internal field using a superimposed AC and DC voltage. It may also be used to observe absorbing species whose populations are modulated by the application of an external voltage, such as polarons. In this case, the sub-gap polaron absorption signal from 1.2 to 1.6 eV (see Figure 4a) is associated with the modulation of the hole doping level by the

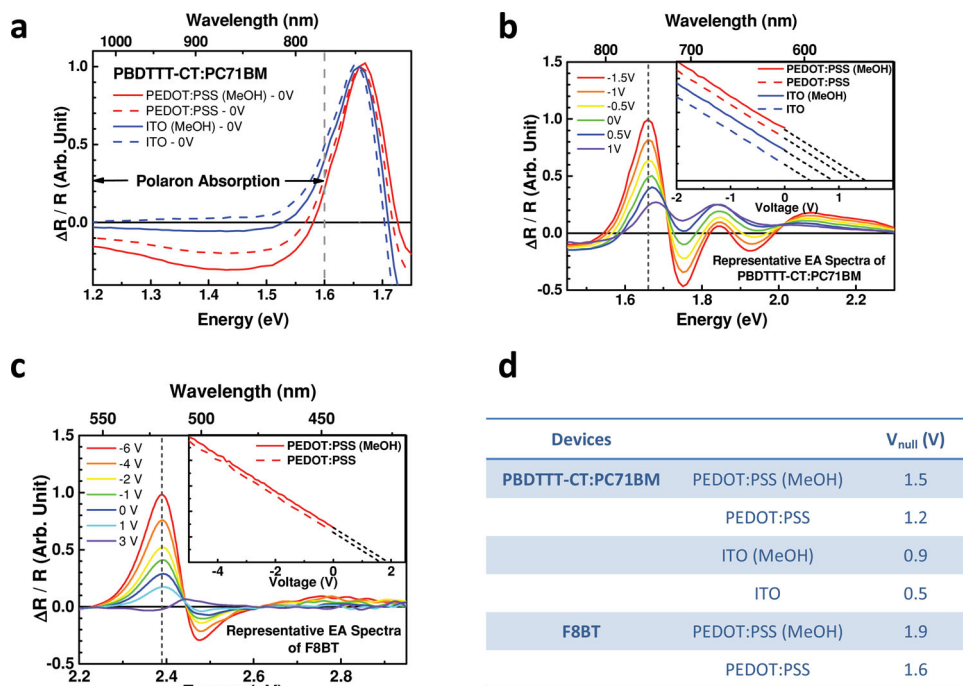


Figure 4. (a) Electroabsorption (EA) spectra of ITO/PEDOT:PSS/PBDTTT-CT:PC71BM/Al and ITO/PBDTTT-CT:PC71BM/Al devices, featuring polaron absorption for methanol treated and control devices. Spectra are normalized at 1.66 eV. (b) Representative EA spectra of PBDTTT-CT:PC71BM photovoltaic device. The inset contains plots of signal amplitude (at 1.66 eV) vs. voltage and V_{null} is obtained from the extrapolated intersection with the x-axis. (c) Representative EA spectra of F8BT PLED device. The inset contains plots of signal amplitude (at 2.38 eV) vs. voltage and V_{null} is obtained from the extrapolated intersection with the x-axis. (d) Table compilation of V_{null} values for PBDTTT-CT:PC71BM and F8BT devices.

AC voltage, and the intensity of this signal is quantitatively proportional to the density of hole doping.^[33] In our devices, the density of hole doping is markedly higher after methanol treatment, consistent with the larger vacuum-level shifts depicted in Figure 3b above. A small amount of hole doping can also be observed in the methanol treated ITO device, suggesting Fermi level pinning and a small vacuum level shift.

The representative EA spectra in Figure 4b and c show the Stark effect signal of PBDTTT-CT and F8BT respectively, and they resemble the first derivative of the polymer π - π^* transition (see Figure S8).^[34,35] In addition to the polaron absorption signal, a positive ground state bleach (GSB) signal, due to hole doping, is seen superimposed on the PBDTTT-CT Stark signal in the range of 1.6 to 2.2 eV. The amplitude of the first harmonic Stark signal is proportional to the DC electric field in the semiconductor active layer. Hence, the Stark signal disappears at zero internal field. This is achieved by applying a DC voltage V_{null} , which gives an estimate of the built-in potential. The Stark signal reverses polarity when the applied DC bias exceeds the built-in potential.^[33,34,36,37] To obtain the built-in potentials of the PBDTTT-CT:PC71BM and F8BT devices, we performed bias dependence EA measurements at 1.66 eV and 2.38 eV photon energy respectively (see insets of Figure 4b,c), where the signal-to-noise ratio is the highest. The EA signal deviates from linearity upon forward bias due to injected charges. Therefore, V_{null} is obtained from the extrapolation of the EA signal from the negative bias regime (see Figure 4d for V_{null} values and Figure S9 for detailed EA spectra).

The built-in potential, as estimated from V_{null} , increased by approximately 0.3 V in all devices upon methanol treatment. The built-in potential is typically determined by the difference in work function between the anode and the cathode, as in a metal-insulator-metal (MIM) model.^[34] The 0.3 V increase in built-in potential is therefore associated with the deepening of anode work function by methanol, consistent with the UPS measurements in Figure 3. For the PEDOT:PSS/PBDTTT-CT:PC71BM/Al device where Fermi level pinning was observed in UPS, the increase in V_{null} is qualitatively consistent with the presence of

an increased local field near the anode interface, which increases the Stark signal from this region in the methanol treated device. The increases in built-in potential and anode work function are consistent with the increases in open-circuit voltage of our photovoltaic devices, as established in the literature.^[2,38]

To investigate the surface molecular mechanism behind the increased work function and the enhanced hole injection/extraction, we directly probed the PBDTTT-CT thin films using multiple reflection attenuated-total-reflectance Fourier transform infrared (ATR-FTIR) spectroscopy. The PBDTTT-CT and PEDOT:PSS/PBDTTT-CT films were spin-coated directly onto Germanium ATR crystals, which were then loaded into an airtight solvent/gas chamber for measurements. The samples were exposed to deuterated methanol (CD_3OD) through solvent injection ports, and the FTIR measurements were taken in-situ, before and after the treatment, to observe for spectral changes. CD_3OD was used to distinguish the solvent spectral features against the polymer IR bands.

Figure 5a shows a schematic diagram of the setup and the conditions that the samples were exposed to at various stages of the ATR-FTIR experiment. The sample chamber was first purged with high purity nitrogen for 30 min to remove ambient gases. A 30 mbar vacuum was then applied for 30 min to remove any volatile solvent species in the polymer film. The chamber was then purged again with nitrogen for 15 min before CD_3OD was injected into the chamber. The CD_3OD was flushed out with nitrogen and the sample was purged dry over 30 min. Vacuum was applied for 30 min to remove any remaining CD_3OD , and the sample was finally flushed with nitrogen for 15 min.

Figure 5b and c show the IR reflectance spectra of Ge/PBDTTT-CT and Ge/PEDOT:PSS/PBDTTT-CT samples at various stages of the in-situ ATR-FTIR experiment. The % reflectance are calculated with respect to the spectral intensity at 0-minute (A) during the nitrogen purge. A reflectance value above the baseline (>100%) represent the loss of an IR absorbing species compared to the film at 0 min, and vice versa. In both samples, spectrum (B) shows that there were no

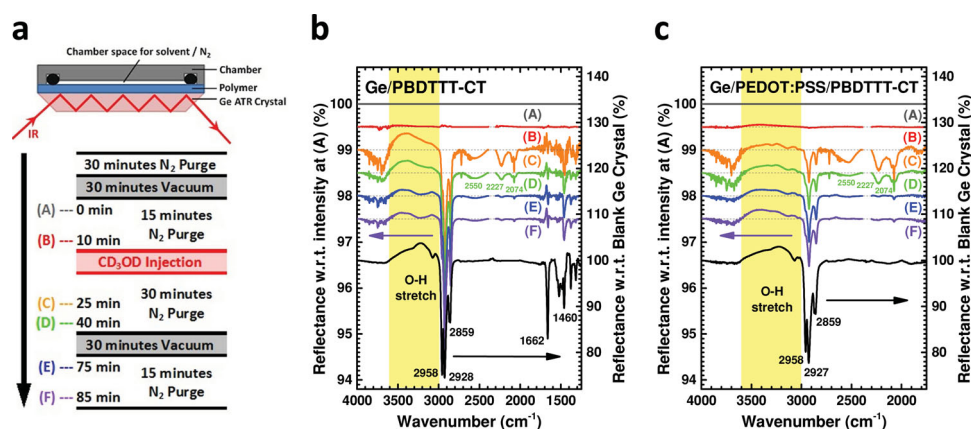


Figure 5. (a) Schematic diagram showing the setup and the processes during the in-situ ATR-FTIR experiments. (b) Reflectance spectra of Ge/PBDTTT-CT and (c) Ge/PEDOT:PSS/PBDTTT-CT at various stages of the in-situ ATR-FTIR experiments. Reflectance spectra (A) to (F), plotted against the left axis, are calculated with respect to spectral intensity at 0 min (A). The spectra are offset by 0.5% for easy comparison. The bottom (black) spectrum, plotted against the right axis, shows the reflectance at 0 min, calculated with respect to spectral intensity measured using a blank Ge ATR-crystal.

changes in the samples during the nitrogen purge before methanol treatment. In spectra (C) to (F), a clear loss of -OH groups could be observed after methanol treatment, as seen from the broad O-H stretching band ($3000\text{--}3600\text{ cm}^{-1}$) above baseline. Interestingly, an increase in IR absorbance of the PBDTTT-CT polymer was observed after methanol treatment, as seen from the characteristic C-H stretching bands ($2958, 2928, 2859\text{ cm}^{-1}$), C=O stretching band (1662 cm^{-1}) and CH_2 bending band (1460 cm^{-1}) of the polymer. Spectrum (E) also shows that deuterated methanol was nearly completely removed after 30 min in vacuum, as seen from the disappearance of C-D stretching bands ($2227, 2074\text{ cm}^{-1}$) and O-D stretching band (2550 cm^{-1}). A similar loss of -OH groups and increase in polymer absorbance can be observed in the samples treated with standard (non-deuterated) methanol (see Figure S10).

We attribute the loss of -OH groups to the removal of surface hydroxyl species by methanol, possibly associated with adsorbed water. This depletion of electron donating hydroxyl groups is consistent with the increases in work function observed on the anode substrates upon methanol treatment.^[39,40] The appearance of polymer IR absorption bands is likely due to the compacting of the polymer film towards the substrate, which will show up as increased absorption because ATR-FTIR is sensitive to the materials closest to the ATR-crystal surface. We propose that the energetic substrate surface, originally adsorbed with polar hydroxyl groups, becomes passivated by the overlying polymer after the hydroxyl groups are displaced during methanol treatment. This would account for better contact between the polymer and the anode substrate surface, decreasing the tunnelling barrier for charges traversing the interface, and thereby provide additional enhancements to charge injection and extraction in devices.

3. Conclusion

We demonstrate that excellent hole injection and extraction can be simultaneously achieved for organic semiconductor devices when the anode work functions are increased by methanol treatment. We also show that the performances of organic solar cells and polymer light-emitting diodes can be significantly improved through this enhancement in charge injection and extraction.

It is surprising that a simple in-situ treatment can lead to such a profound change in the properties of the device, and suggests that the possibility of similar effects arising from other wet processing techniques should not be discounted. However, the ability to specifically target and modify a single interface within a device, leaving all other components unaffected, presents a uniquely powerful tool for device engineering. This work distinctly highlights the critical role that interfaces play in determining device performance,^[6,41] and the clear understanding of the physical and molecular mechanisms behind non-solvent treatment offers scope for the future implementation of similar processes in interface optimization and device enhancement.

4. Experimental Section

Materials: PBDTTT-CT (Solarmer Materials Inc.), PC71BM (Solenne BV), F8BT (Cambridge Display Technology) and PEDOT:PSS (Heraeus, Clevis P VP Al 4083) were used as received.

Photovoltaic Device Fabrication: ITO-coated glass substrates were cleaned by successive sonication in acetone and isopropanol, followed by oxygen plasma treatment. PEDOT:PSS ($\sim 30\text{ nm}$) was spin-coated onto the substrate, followed by heat annealing at $120\text{ }^\circ\text{C}$ for 30 min under nitrogen atmosphere. A 37.5 mg/mL solution of PBDTTT-CT:PC71BM blend (1:1.5 ratio) in chlorobenzene with 3 v% diiodooctane was spin-coated on the prepared substrate to give a $\sim 100\text{ nm}$ film. For the methanol treated samples, methanol was dispensed onto the blend film and allowed to stand for 15 seconds before spinning dry. A 100 nm layer of aluminium was deposited by thermal evaporation under high vacuum ($\sim 10^{-6}\text{ mbar}$). All devices were encapsulated under glass before device characterization in air.

PLED Device Fabrication: The LED substrates were prepared as for the PV substrates. A 25 mg/mL solution of F8BT in p-xylene was spin-coated on the prepared substrate to give a $\sim 200\text{ nm}$ film. F8BT-coated substrates were annealed in a nitrogen-filled glovebox for 20 minutes at $155\text{ }^\circ\text{C}$. For the methanol treated samples, methanol was dispensed onto the film and allowed to stand for 30 s before spinning dry. A 100 nm layer of aluminium was deposited by thermal evaporation under high vacuum ($\sim 10^{-6}\text{ mbar}$). All devices were encapsulated under glass before device characterization in air.

Hole-only Device Fabrication: All device substrates were prepared as for the PV substrates. For hole-only devices of PBDTTT-CT:PC71BM blend, the active layer (95 nm) was prepared as described in 'Photovoltaic Device Fabrication'. For pure PBDTTT-CT devices, a 40 mg/mL solution of PBDTTT-CT in chlorobenzene was spin-coated on the substrate to give a 130 nm film. For F8BT devices, a 25 mg/mL solution of F8BT in p-xylene was spin-coated on the substrate to give a 210 nm film. For the methanol treated samples, methanol was dispensed onto the film and allowed to stand for 15 s before spinning dry. MoO_3 (5 nm) and Ag (100 nm) were sequentially deposited by thermal evaporation under high vacuum ($\sim 10^{-6}\text{ mbar}$). All devices were encapsulated under glass before device characterization in air.

Photovoltaic Device Characterization: The device current-voltage characteristics, under the illumination of an Oriol 81160-1000 solar simulator, were measured using a Keithley 2635 Source Measure Unit (SMU). The solar simulator was calibrated with a silicon reference solar cell, to give an equivalent illumination intensity of $100\text{ mW cm}^{-2}\text{ AM} 1.5\text{G}$, after correction for spectral mismatch.

PLED Device Characterization: Current-voltage characteristics were measured using a Keithley 2400 SMU acting as a voltage source, while luminance was detected simultaneously using a silicon photodiode centred over the driven pixel. Luminance in candela was calculated assuming a Lambertian emission profile, and from the known emission spectrum of F8BT and the known spectral response of the photodiode.

Transient Photocurrent: A 525 nm green LED and a Hewlett Packard (HP) 8116A function generator was used to create $10\text{ }\mu\text{s}$ width square light pulses at a frequency of 20 kHz . Short-circuit photocurrent transients were measured using an Agilent DSO6052A digitizing oscilloscope with an input impedance of $50\text{ }\Omega$. Photocurrent transients at forward bias were measured while another HP 8116A function generator was connected across the device as a constant voltage source.

Ultraviolet Photoelectron Spectroscopy: The UPS samples were prepared on ITO glass substrates as described in the device fabrication section and transferred to the ultrahigh vacuum (UHV) chamber (ESCALAB 250Xi) for measurements. UPS measurements were performed using a double-differentially pumped He gas discharge lamp emitting He I radiation ($h\nu = 21.22\text{ eV}$) with a pass energy of 2 eV .

Electroabsorption Spectroscopy: A superposition of DC and AC voltages was applied to the test device while the device was illuminated with a 150 W xenon arc lamp (Oriol 6253), passed through a Bruker Optics 250is/sm Imaging Spectrograph/Scanning monochromator. The change in the reflected probe light intensity, ΔR , was monitored by an OPT 301 silicon photodiode and recorded with a dual channel lock-in amplifier (SR830 Stanford Research Systems). The DC component of the light intensity, R , was measured by a HP34401A digital multimeter.

ATR-FTIR: The Germanium ATR-crystal substrates were cleaned by successive sonication in acetone and isopropanol, followed by oxygen

plasma treatment. In one sample, PEDOT:PSS (~30 nm) was spin-coated onto the substrate, followed by heat annealing at 120 °C for 30 min under nitrogen atmosphere. A thin layer of PBDTTT-CT (~80 nm) was spin-coated onto the prepared substrate. The in-situ ATR-FTIR measurements were performed as described in the main text, using a PerkinElmer Spectrum 100 FTIR spectrometer.

Supporting Information

Supporting Information is available from the Wiley Online Library or from the author.

Acknowledgements

We thank the EPSRC (UK) for financial support. Z. K. T. thanks the Singapore National Research Foundation (Energy Innovation Programme Office) for the research scholarship. D. C. thanks Cambridge Display Technology for financial support. C. L. thanks Chinese Scholarship Council (CSC) for financial support. The authors thank Prof. Paul B. Davies, Prof. Ullrich Steiner and Prof. Ulrich Wiesner for their insights and useful discussions. We thank Dr. Paul Hopkinson, Reza Saberi Moghaddam and Carlo Tarantini for their experimental help and useful discussions. Part of this work is based on research conducted at beamline D1 at the Cornell High Energy Synchrotron Source (CHESS). We thank D.-M. Smilgies, Ernie Fontes, Margaret Koker, Joerg Werner and Hiroaki Sai for their help during the D1 experiment at CHESS.

Received: October 4, 2013

Revised: November 26, 2013

Published online: February 12, 2014

- [1] P. W. M. Blom, V. D. Mihailetschi, L. J. A. Koster, D. E. Markov, *Adv. Mater.* **2007**, *19*, 1551.
- [2] C. J. Brabec, A. Cravino, D. Meissner, N. S. Sariciftci, T. Fromherz, M. T. Rispens, L. Sanchez, J. C. Hummelen, *Adv. Funct. Mater.* **2001**, *11*, 374.
- [3] Y. Shen, A. R. Hosseini, M. H. Wong, G. G. Malliaras, *ChemPhys Chem* **2004**, *5*, 16.
- [4] P. K. H. Ho, J.-S. Kim, J. H. Burroughes, H. Becker, S. F. Y. Li, T. M. Brown, F. Cacialli, R. H. Friend, *Nature* **2000**, *404*, 481.
- [5] L. S. Hung, C. W. Tang, M. G. Mason, *Appl. Phys. Lett.* **1997**, *70*, 152.
- [6] Y. Zhou, C. Fuentes-Hernandez, J. Shim, J. Meyer, A. J. Giordano, H. Li, P. Winget, T. Papadopoulos, H. Cheun, J. Kim, M. Fenoll, A. Dindar, W. Haske, E. Najafabadi, T. M. Khan, H. Sojoudi, S. Barlow, S. Graham, J.-L. Brédas, S. R. Marder, A. Kahn, B. Kippelen, *Science* **2012**, *336*, 327.
- [7] T. Shizuo, N. Koji, T. Yasunori, *J. Phys. D: Appl. Phys.* **1996**, *29*, 2750.
- [8] Y. Zhang, P. W. M. Blom, *Appl. Phys. Lett.* **2011**, *98*, 143504.
- [9] L.-P. Lu, D. Kabra, K. Johnson, R. H. Friend, *Adv. Funct. Mater.* **2012**, *22*, 144.
- [10] M. Vasilopoulou, L. C. Palilis, D. G. Georgiadou, S. Kennou, I. Kostis, D. Davazoglou, P. Argitis, *Appl. Phys. Lett.* **2012**, *100*, 013311.
- [11] M. C. Gwinner, R. D. Pietro, Y. Vaynzof, K. J. Greenberg, P. K. H. Ho, R. H. Friend, H. Sirringhaus, *Adv. Funct. Mater.* **2011**, *21*, 1432.
- [12] J. Meyer, S. Hamwi, T. Bulow, H.-H. Johannes, T. Riedl, W. Kowalsky, *Appl. Phys. Lett.* **2007**, *91*, 113506.
- [13] J. Luo, H. Wu, C. He, A. Li, W. Yang, Y. Cao, *Appl. Phys. Lett.* **2009**, *95*, 043301.
- [14] Z. He, C. Zhong, X. Huang, W.-Y. Wong, H. Wu, L. Chen, S. Su, Y. Cao, *Adv. Mater.* **2011**, *23*, 4636.
- [15] J. H. Seo, A. Gutacker, Y. Sun, H. Wu, F. Huang, Y. Cao, U. Scherf, A. J. Heeger, G. C. Bazan, *J. Am. Chem. Soc.* **2011**, *133*, 8416.
- [16] Y.-M. Chang, R. Zhu, E. Richard, C.-C. Chen, G. Li, Y. Yang, *Adva. Funct. Mater.* **2012**, *22*, 3284.
- [17] J. Fang, B. H. Wallikewitz, F. Gao, G. Tu, C. Müller, G. Pace, R. H. Friend, W. T. S. Huck, *J. Am. Chem. Soc.* **2010**, *133*, 683.
- [18] Q. Wang, Y. Zhou, H. Zheng, J. Shi, C. Li, C. Q. Su, L. Wang, C. Luo, D. Hu, J. Pei, J. Wang, J. Peng, Y. Cao, *Org. Electronics* **2011**, *12*, 1858.
- [19] S. Nam, J. Jang, H. Cha, J. Hwang, T. K. An, S. Park, C. E. Park, *J. Mater. Chem.* **2012**, *22*, 5543.
- [20] X. Liu, W. Wen, G. C. Bazan, *Adv. Mater.* **2012**, *24*, 4505.
- [21] H. Zhou, Y. Zhang, J. Seifert, S. D. Collins, C. Luo, G. C. Bazan, T.-Q. Nguyen, A. J. Heeger, *Adv. Mater.* **2013**, *25*, 1646.
- [22] L. Huo, S. Zhang, X. Guo, F. Xu, Y. Li, J. Hou, *Angew. Chem. Int. Ed.* **2011**, *50*, 9697.
- [23] N. F. Mott, R. W. Gurney, *Electronic Processes in Ionic Crystals*, Clarendon Press, Oxford **1948**.
- [24] P. N. Murgatroyd, *J. Phys. D: Appl. Phys.* **1970**, *3*, 151.
- [25] C. G. Shuttle, B. O'Regan, A. M. Ballantyne, J. Nelson, D. D. C. Bradley, J. R. Durrant, *Phys. Rev. B* **2008**, *78*, 113201.
- [26] L. J. A. Koster, E. C. P. Smits, V. D. Mihailetschi, P. W. M. Blom, *Phys. Rev. B* **2005**, *72*, 085205.
- [27] H. J. Bolink, E. Coronado, D. Repetto, M. Sessolo, E. M. Barea, J. Bisquert, G. Garcia-Belmonte, J. Prochazka, L. Kavan, *Adv. Funct. Mater.* **2008**, *18*, 145.
- [28] K. Murata, S. Cina, N. C. Greenham, *Appl. Phys. Lett.* **2001**, *79*, 1193.
- [29] T. van Woudenberg, J. Wildeman, P. W. M. Blom, J. J. A. M. Bastiaansen, B. M. W. Langeveld-Vos, *Adv. Funct. Mater.* **2004**, *14*, 677.
- [30] C. Tengstedt, W. Osikowicz, W. R. Salaneck, I. D. Parker, C.-H. Hsu, M. Fahlman, *Appl. Phys. Lett.* **2006**, *88*, 053502.
- [31] S. Braun, W. Osikowicz, Y. Wang, W. R. Salaneck, *Org. Electronics* **2007**, *8*, 14.
- [32] Z. Xu, L.-M. Chen, M.-H. Chen, G. Li, Y. Yang, *Appl. Phys. Lett.* **2009**, *95*, 013301.
- [33] M. Zhou, L.-L. Chua, R.-Q. Png, C.-K. Yong, S. Sivaramakrishnan, P.-J. Chia, A. T. S. Wee, R. H. Friend, P. K. H. Ho, *Phys. Rev. Lett.* **2009**, *103*, 036601.
- [34] I. H. Campbell, T. W. Hagler, D. L. Smith, J. P. Ferraris, *Phys. Rev. Lett.* **1996**, *76*, 1900.
- [35] G. U. Bublitz, S. G. Boxer, *Annu. Rev. Phys. Chem.* **1997**, *48*, 213.
- [36] T. M. Brown, R. H. Friend, I. S. Millard, D. J. Lacey, J. H. Burroughes, F. Cacialli, *Appl. Phys. Lett.* **2001**, *79*, 174.
- [37] P. A. Lane, J. C. deMello, R. B. Fletcher, M. Bernius, *Appl. Phys. Lett.* **2003**, *83*, 3611.
- [38] V. D. Mihailetschi, L. J. A. Koster, P. W. M. Blom, *Appl. Phys. Lett.* **2004**, *85*, 970.
- [39] F. Nuesch, L. J. Rothberg, E. W. Forsythe, Q. T. Le, Y. Gao, *Appl. Phys. Lett.* **1999**, *74*, 880.
- [40] N. Koch, A. Vollmer, A. Elschner, *Appl. Phys. Lett.* **2007**, *90*, 043512.
- [41] M. Graetzel, R. A. J. Janssen, D. B. Mitzi, E. H. Sargent, *Nature* **2012**, *488*, 304.